Coaxial and Circular Waveguide Bandpass Filters using Printed Metal Inserts

B. Varailhon de la Filolie and R. Vahldieck

Laboratory for Lightwave Electronics, Microwaves and Communications
(LLiMiC)
Department of Electrical and Computer Engineering
University of Victoria
Victoria, B.C., V8W 3P6, Canada

Abstract

This paper presents a field theoretical analysis of metal septum loaded coaxial and circular waveguide sections. Based on the s-parameters derived from this analysis, bandpass filters are designed for the 30 GHz range. Theoretical performance and measured results are in excellent agreement and are better than 1.3 dB (S_{21}) and 25 dB (S_{11}), respectively.

Introduction

Coaxial and circular waveguide technology is used at higher frequencies with ever shrinking guide dimensions. The design and fabrication of filters at these frequencies requires accurate theoretical tools and manufacturing methods since fine tuning of these filters is a difficult task.

In this paper, we describe the use of ladder shaped metal insert filters to be used in circular split block housing and coaxial waveguides (Fig. 1). In particular, the combination of printed metal inserts with coaxial transmission lines is a new and interesting approach for mechanically stable and high performance coaxial bandpass filters. The basic idea is derived from the E-plane filter design, which was successfully used in rectangular waveguides up to 170GHz [1].

The theoretical design of the circular and coaxial waveguide filters is based on a field theoretical description of the scattering parameters for the discontinuities shown in Fig. 2. The analysis includes TE-TM mode coupling and the metal septum is approximated by a bow-tie shaped structure. This approximation is necessary to avoid θ-dependent boundary conditions, which is the case if a rectangular discontinuity were used. Thus, it is possible to use only Bessel eigenfunctions in all waveguide subsections and the coupling integrals, which are resulting from the field matching at the transition, can be solved analytically. This makes the design algorithm relatively fast, and, as will be discussed later, does not introduce a noticeable deviation of the practical filter response from the theoretically predicted one.

Theory

As explained before, to avoid coupling integrals composed of eigenfunctions of different coordinates systems, the septum is represented by a bow-tie shaped discontinuity. In both types of filters, any incident waves at the abrupt transition from a standard circular or coaxial waveguide to the bifurcated waveguide section can excite TE^s, TE^c, TM^s and TM^c modes in region (1), as well as a TM_{00} mode (equivalent to the TEM mode) in the coaxial case, and TE and TM modes in regions (2) and (3) (see Fig. 2), respectively. The superscripts s and c indicate, respectively, the sine (E-field perpendicular to the septum) and cosine (E-field parallel to the septum) polarizations.

Defining the potential vectors $\Psi^{(e,h)}$ in each subregions, the electric and magnetic fields can be written as:

$$\vec{E} = -\vec{\nabla}\times\vec{\Psi}^{(h)} + \frac{1}{j\omega\varepsilon}\vec{\nabla}\times\vec{\nabla}\times\vec{\Psi}^{(e)}$$

$$\vec{H} = \vec{\nabla}\times\vec{\Psi}^{(e)} + \frac{1}{j\omega\mu}\vec{\nabla}\times\vec{\nabla}\times\vec{\Psi}^{(h)}$$

$\Psi(\rho,\theta,z)$ must, in each subsection, satisfy the cylindrical Helmholtz equation and the boundary condition. This leads to the following expression for the E- and H-field:

$$\vec{E}_T = -\frac{1}{\omega\varepsilon}\sum_{n=0}^{\infty}\sum_{m=1}^{\infty}\beta_{n,m}^{(e)}T_{n,m}^{(e)}\left(A_{n,m}+B_{n,m}\right)\vec{e}_{n,m}^{(e)} - \sum_{p=0}^{\infty}\sum_{q=s}^{\infty}T_{p,q}^{(h)}\left(C_{p,q}+D_{p,q}\right)\vec{e}_{p,q}^{(h)}$$

$$\vec{H}_T = \sum_{n=0}^{\infty}\sum_{m=1}^{\infty}T_{n,m}^{(e)}\left(A_{n,m}-B_{n,m}\right)\vec{h}_{n,m}^{(e)} + \frac{1}{\omega\mu}\sum_{p=0}^{\infty}\sum_{q=s}^{\infty}\beta_{p,q}^{(h)}T_{p,q}^{(h)}\left(C_{p,q}-D_{p,q}\right)\vec{h}_{p,q}^{(h)}$$

where $(e^{(e)})_{n,m}$ and $(e^{(h)})_{p,q}$ are two sets of orthonormal functions (see appendix for the sets in subregions (2) and (3)). The upper index (e) and (h) specifies the TM and TE mode, respectively. The parameter s is set according to the type of guide:

s=1	in the circular waveguide
s=0	in the coaxial cable (corresponding to TEM mode).

β denotes the propagation constant :

$$\beta_{n,m}^{(e,h)2} = k_0^2 - k_{n,m}^{(e,h)2}$$

and $k^{(e)}$ (resp. $k^{(h)}$) are the wave numbers which are the zero's of the function $F(k^{(e)}b)$ (resp. $F'(k^{(h)}b)$), defined in the appendix. The constant T is obtained by normalizing the power to 1 W. $A_{n,m}$ and $C_{p,q}$ are the forward wave amplitudes for the TM and TE modes, respectively, and $B_{n,m}$ and $D_{p,q}$ are the reflected wave amplitudes for the TM and TE modes, respectively.

At the interface (z=0) of the bifurcation, the E-field continuity condition yields:

IF2

$$\vec{E}_T^{(1)} = \vec{E}_T^{(2)} \qquad \theta \in [\gamma, \pi - \gamma]$$
$$= \vec{E}_T^{(3)} \qquad \theta \in [\pi + \gamma, 2\pi - \gamma]$$
$$= 0 \qquad \theta \in [0, \gamma],\ \theta \in [\pi - \gamma, \pi + \gamma] \text{ and } \theta \in [2\pi - \gamma, 2\pi]$$

And similarly for the H-field:

$$\vec{H}_T^{(1)} = \vec{H}_T^{(2)} \qquad \theta \in [\gamma, \pi - \gamma]$$
$$= \vec{H}_T^{(3)} \qquad \theta \in [\pi + \gamma, 2\pi - \gamma]$$

To separate the amplitude coefficients in both equations, we utilize the orthogonality property between modes in region (1) for the E-field and in region (2) and (3) for the H-field as follows [1]:

$$\int_{S_1} \vec{E}_T^{(1)} . e\, w(\rho,\theta) dS = \int_{S_2} \vec{E}_T^{(2)} . e\, w(\rho,\theta) dS + \int_{S_3} \vec{E}_T^{(3)} . e\, w(\rho,\theta) dS$$

where **e** is the appropriate set of eigen-vectors and w the weight function. A similar set of equations can be obtained for the H-field.

Rearranging the resulting equations, we are able to express all reflected wave amplitude coefficients as a function of the incident wave amplitude coefficients. This constitutes the three port s-matrix of the bifurcation:

$$\begin{pmatrix} B^{(1)} \\ A^{(2)} \\ A^{(3)} \end{pmatrix} = \begin{pmatrix} S_{11} & S_{12} & S_{13} \\ S_{21} & S_{22} & S_{23} \\ S_{31} & S_{32} & S_{33} \end{pmatrix} \begin{pmatrix} A^{(1)} \\ B^{(2)} \\ B^{(3)} \end{pmatrix}$$

The septum loaded circular waveguide is a reciprocal network. Therefore, knowing the s-matrix at one side of the discontinuity, the s-matrix at the opposite side is known too. Then, by including the effect of the finite length of the septum, both s-matrices are combined to give the overall two port s-matrix of the septum. In the next step, the septum s-matrices are cascaded by separating each with a uniform circular waveguide of length L_i (the resonator section) to give the overall s-matrix of the filter.

Results

A convergence analysis of a finite length septum shows that a minimum of 40 TE and TM modes are necessary for acceptable convergence. This computation includes all modes (e.g. sine and cosine, TE and TM modes). Nevertheless, for small angle (less than 10 degrees), the coupling between TE and TM modes is negligible. Therefore, assuming a TE mode incident wave, the analysis in the passband can be done only with TE mode. This assumption is not valid any longer close to the cutoff frequency of the first propagating TM mode or for angles greater than 10 degrees. In these cases, all modes should be considered to obtain accurate results (see Fig.3).

Fig. 3 shows the theoretical and measured performance of a five resonator Ka-Band filter in a 4 mm diameter circular waveguide. The filter structure is composed of a series of resonant cavities separated by coupling septa. The initial filter was synthesized with lumped element theory [2]. From these element values, s-parameters were calculated from which the corresponding insert dimensions can be derived. However, since the higher-order mode interaction between subsequent discontinuities is not included in the lumped elements synthesis, the initial filter response was off by 1 GHz. Nevertheless, these insert dimensions were only used as start values for the full wave analysis and the generalized s-matrix of the entire filter was optimized using the optimization procedure in [1].

The measured insertion loss is less than 1.3 dB in the passband (0.1 dB computed) while the respective return loss is greater than 22 dB (25 dB computed). The reflection coefficient for the polarization perpendicular to the septum is greater than 30 dB (35 dB computed) over the operating range (26 to 40 GHz), which indicates a good decoupling between both polarizations. Thus, the approximation of the planar structure by a bow-tie shape does not lead to noticeable discrepancies between theory and measurements.

Fig. 4 shows the performance of a three resonators K-Band filter in a standard SMA coaxial guide. The structure is similar to the circular waveguide filter. A TEM mode incident wave is assumed. The computed insertion loss is less than 0.1 dB in the passband. The computed reflection coefficient is better than 35 dB in the same band.

Conclusion

This paper has presented a design method for metal insert filters in circular or coaxial waveguides. Approximating the rectangular septum by a bow-tie shape, the numerical procedure is simplified due to the easier handling of the boundary conditions. This step does not introduce a noticeable error between theory and measurements. Fabrication is made easy due the applicability of low-cost photolithographic techniques. The filter realization did not require any physical fine tuning.

Appendix

1) E-field orthonormalized vectors in region (2):

•TM mode (at z=0):

$$\vec{e}_{n,m}^{(e)} = \alpha_{n,m}^{(e)} \left[\sin(r(\theta-\gamma)) \frac{dF(k_{n,m}^{(e)}\rho)}{d\rho} \vec{\rho} + \frac{r}{\rho} \cos(r(\theta-\gamma)) F(k_{n,m}^{(e)}\rho) \vec{\theta} \right]$$

•TE mode (at z=0):

$$\vec{e}_{p,q}^{(h)} = \alpha_{p,q}^{(h)} \left[-\frac{r}{\rho} \sin(r(\theta-\gamma)) F(k_{p,q}^{(h)}\rho) \vec{\rho} - \cos(r(\theta-\gamma)) \frac{dF(k_{p,q}^{(h)}\rho)}{d\rho} \vec{\theta} \right]$$

2) H-field orthonormalized vectors:

•TM mode (at z=0):

$$\vec{h}_{n,m}^{(e)} = \alpha_{n,m}^{(e)} \left[\frac{r}{\rho} \cos(r(\theta-\gamma)) F(k_{n,m}^{(e)}\rho) \vec{\rho} - \sin(r(\theta-\gamma)) \frac{dF(k_{n,m}^{(e)}\rho)}{d\rho} \vec{\theta} \right]$$

•TE mode (at z=0):

$$\vec{h}_{p,q}^{(h)} = -\alpha_{p,q}^{(h)} \left[\sin(r(\theta-\gamma)) \frac{dF(k_{p,q}^{(h)}\rho)}{d\rho} \vec{\rho} + \frac{r}{\rho} \cos(r(\theta-\gamma)) F(k_{p,q}^{(h)}\rho) \vec{\theta} \right]$$

the coefficients α being the orthonormalized factor. The F function depends of the type of guide:

$$F(k_{n,m}^{(e)}\rho) = N_r(k_{n,m}^{(e)}b) J_r(k_{n,m}^{(e)}\rho) - J_r(k_{n,m}^{(e)}b) N_r(k_{n,m}^{(e)}\rho)$$
$$F(k_{p,q}^{(h)}\rho) = N_r'(k_{p,q}^{(h)}b) J_r(k_{p,q}^{(h)}\rho) - J_r'(k_{p,q}^{(h)}b) N_r(k_{p,q}^{(h)}\rho)$$

in the coaxial guide and

$$F\left(k_{n,m}^{(e,h)}\rho\right) = J_r\left(k_{n,m}^{(e,h)}\rho\right)$$

in the circular waveguide.The fields in regions (3) are obtained by replacing $(\theta-\gamma)$ by $(\theta-\pi-\gamma)$. r is defined as:

$$r = n\frac{\pi}{\pi - 2\gamma}$$

References

1. R. Vahldieck, J. Bornemann, F. Arndt and D. Grauerholz, "Optimized Waveguide E-Plane Metal Insert Filters for Millimeter-Wave Applications", IEEE Trans. Microwave Theory and Tech., vol. MTT-31, Jan. 1983, pp. 65-69.

2 L. Q. Bui, D. Ball and T. Itoh, "Broadband Millimeter-Wave E-Plane Bandpass Filters", IEEE MTT, International Microwave Symp. Digest, 1984, pp. 236-240.

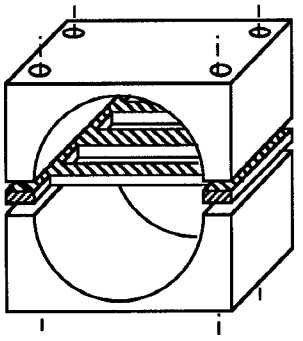

a) Circular Waveguide Filter

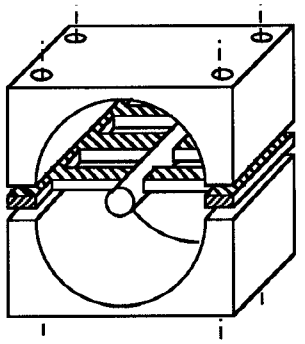

b) Coaxial Filter

Fig.1 Structure of the Metal Insert Filter

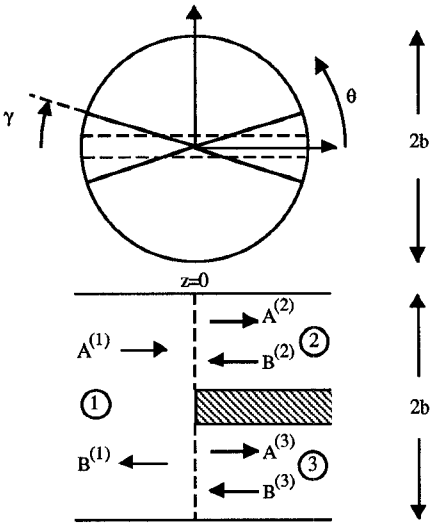

a) Circular Waveguide configuration

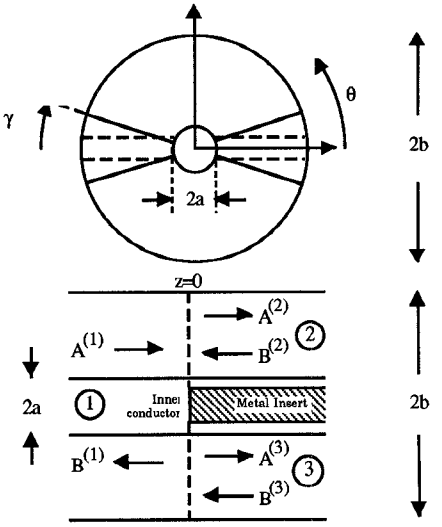

b) Coaxial configuration

Fig. 2 details of the bow-tie shaped abrupt transition

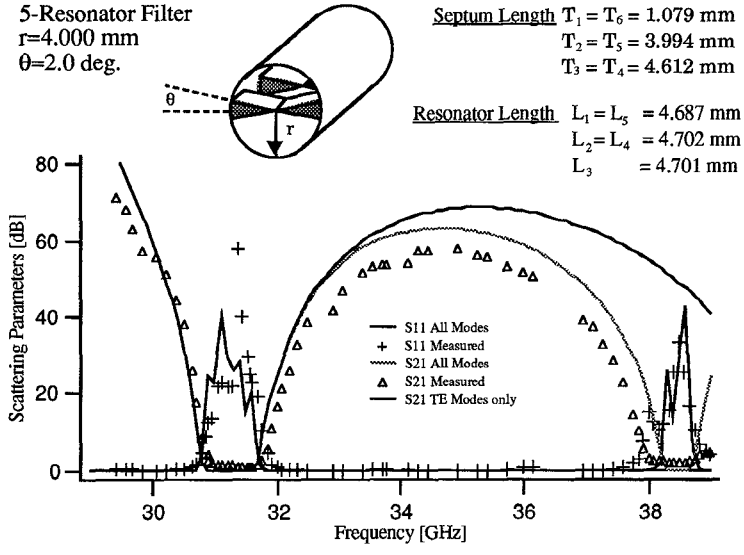

Fig.3: Performance versus Frequency of a 5-Resonator Circular Waveguide Filter

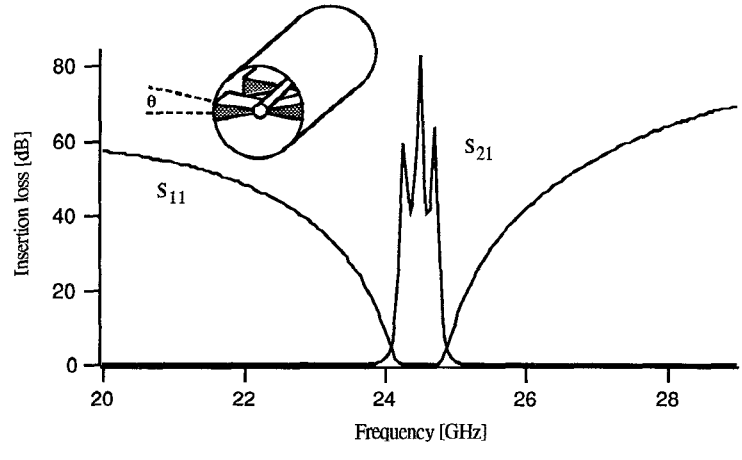

Fig.4: Performance versus frequency of a 3-Resonator Coax Filter